Estimating the Gross Moist Stability of the Tropical Atmosphere*

JIA-YUH YU

Department of Atmospheric Sciences, Chinese Culture University, Yang-Ming Shan, Taipei, Taiwan

CHIA CHOU

Department of Atmospheric Sciences, University of California, Los Angeles, Los Angeles, California

J. DAVID NEELIN

Department of Atmospheric Sciences and Institute of Geophysics and Planetary Physics, University of California, Los Angeles, Los Angeles, California

(Manuscript received 4 November 1996, in final form 30 July 1997)

ABSTRACT

Recent theoretical studies have indicated that large-scale circulation in deep convective regions evolves subject to an overall static stability—termed the gross moist stability—that takes into account both dry static stability and moist convective effects. The gross moist stability has been explicitly defined for a continuously stratified atmosphere under convective quasi-equilibrium constraints. A subsidiary quantity—the gross moisture stratification—measures the overall effectiveness in producing precipitation subject to these quasi-equilibrium constraints. These definitions are relevant in regions that experience deep convection sufficiently often; criteria based on climatological precipitation and maximum level of convection are used to define a domain of applicability. In this paper, 10-yr monthly mean rawinsonde data, and European Centre for Medium-Range Weather Forecasts (ECMWF) and National Meteorological Center (NMC) analyses are used to estimate the magnitude and horizontal distribution of these two quantities in the Tropics within the domain of applicability.

The gross moist stability is found to be positive but much smaller than typical dry static stability values. Its magnitude varies modestly from 200 to 800 J kg^{-1} and exhibits relatively little dependence on sea surface temperature (SST). These values correspond, for instance, to a phase speed change from 8 to 16 m s^{-1} for the Madden–Julian oscillation. The gross moisture stratification is larger and exhibits strong dependence on SST, varying from 1500 to 3500 J kg^{-1} between cold and warm SST regions. A high degree of cancellation between effects of increasing low-level moisture and maximum level of convection, respectively, tends to keep the gross moist stability values relatively constant. Differences among the ECMWF and NMC analysis products and the rawinsonde data affect the estimate, but there is qualitative agreement. It is encouraging that reasonably robust estimates of a small, positive gross moist stability (as the difference between larger dry static stability and gross moisture stratification quantities) can be obtained. This helps justify use of small, constant moist phase speeds in some simple models of tropical circulation, although it also points out inconsistencies in how such models neglect variations in the height of convection.

1. Introduction

In the Tropics, it has long been recognized that the appearance of organized deep convection is strongly associated with high sea surface temperature (SST) and surface wind convergence (Gutzler and Wood 1990; Fu et al. 1990; Waliser et al. 1993; Zhang 1993; Fu et al. 1994). Meanwhile, the latent heat release in tropical deep convection regions serves as the main energy source for many large-scale features, such as the ITCZ (intertropical convergence zone) and the MJO (Madden–Julian oscillation). The interaction between the ensemble effects of deep convection and the large-scale circulation, and the link between these and ocean surface conditions, is a longstanding issue in tropical studies. This has been studied in number of simple models. Despite the apparent diversity of the proposed mechanisms in linking SST to convection and large-scale circulation, these simple models all have some degree of success in simulating the low-level flow forced by SST anomalies. In such studies, the latent heating is either directly coupled to the SST (e.g., Gill 1980; Weare 1986; Kleeman 1991; and many others) or indirectly linked to the SST

* University of California, Los Angeles, IGPP Contribution Number 4712.

Corresponding author address: J. David Neelin, Department of Atmospheric Sciences, University of California, Los Angeles, Los Angeles, CA 90095-1565.
E-mail: neelin@atmos.ucla.edu

through a simple feedback mechanism (e.g., Zebiak 1982, 1986; Webster 1981). Lindzen and Nigam (1987) bypassed treating the explicit effect of latent heating and suggested that the SST affects the atmospheric boundary layer by changing baroclinic pressure gradients. Neelin and Held (1987) modeled time-mean, large-scale deep convection features in the Tropics by using the vertically integrated moist static energy budget in a two-layer model. They suggested that a quantity termed the ''gross moist stability'' is important to large-scale motions in convective regions. In a two-layer model, this is just the difference between the dry static stability and the lower-layer moisture. If the lower-layer moisture increases with SST and dry static stability is constant, the two-layer model gives small gross moist stability in regions of high SST and thus favors convergence zones. A similar two-layer model was also applied to a time-dependent case (Neelin et al. 1987).

Recently, in a more formal framework, Neelin and Yu (1994, hereafter NY) carried out a series of analytical solutions in a continuously stratified atmosphere to discuss the modes of tropical variability arising through the interaction between the large-scale dynamics and cumulus convection using the Betts–Miller (Betts 1986; Betts and Miller 1986) moist convective adjustment (MCA) scheme. The quasi-equilibrium (QE) constraints implied by the Betts–Miller MCA scheme lead to a precise definition of the gross moist stability, referred to here by the symbol M. Under the same framework, Yu and Neelin (1997) demonstrated that the methods applied in NY (i.e., the convective QE constraints) can be carried over to a model that refines the Neelin–Held mechanism with a more precise definition of the gross moist stability that allows continuous stratification, horizontal inhomogeneity, and variations of the depth of convection. They further pointed out that different mechanisms proposed in many simple models, such as the Lindzen–Nigam and Neelin–Held mechanisms, are to a large extent reconcilable. The gross moist stability measures the net stability, including the moisture effects, of the atmosphere felt by the large-scale perturbations. For the time-dependent case, M dictates the phase speed of the low-frequency MJO (NY). For the steady-state case, it affects the nonlocal atmospheric response since this is determined by the balance between damping terms and the propagation tendency of equatorially trapped waves associated with M (Yu and Neelin 1997). A ''gross moisture stratification'' can also be internally defined through the moisture budget under the same QE constraints. This quantity characterizes the moisture available for precipitation in presence of large-scale convergence.

Many studies (Lau and Peng 1987; Lau and Shen 1988; Swinbank et al. 1988; Hess et al. 1993; Waliser et al. 1993) have also shown that the strength of the MJO and the ITCZ can be significantly modulated by SST, with stronger response over warmer ocean. For reference, Fig. 1 displays the observed seasonal cycle of SST and precipitation in the Tropics. Regions with heavy precipitation are associated with warmer SST but not perfectly.

Although theoretical results suggest that the gross moist stability and the gross moisture stratification are important, there has been almost no work on estimating them. In this paper, spatial distributions of both gross moist stability and gross moisture stratification are estimated using rawinsonde data and analysis data of the global tropics from the European Centre for Medium-Range Weather Forecasts (ECMWF) and the National Meteorological Center (NMC, now the National Centers for Environmental Prediction). In section 2, formulation of the gross moist stability is presented. Section 3 briefly describes the datasets used. Section 4 presents estimates of the gross moist stability, gross moisture stratification, and a comparison of the results between ECMWF and rawinsonde datasets (results based on NMC data are presented in appendix B). Section 5 provides an analytical examination of factors affecting the gross moist stability using two idealized cases. Further analysis using ECMWF data is also included in this section. Section 6 discusses the physical implications of the results. Conclusions are summarized in section 7.

2. Formulation

A precise definition of the gross moist stability was first presented in NY for the case of a homogeneous convective atmosphere. Later, Yu and Neelin (1997) generalized to the case of slowly varying basic states. Under the same framework, this also leads to a precise definition of the gross moisture stratification through the moisture budget. We note that both quantities are internally defined in a continuously stratified atmosphere under deep convective QE constraints. We summarize definitions of these two quantities here. A brief outline of the Yu and Neelin (1997) derivation is presented in appendix A for reference.

The gross moist stability (M) and the gross moisture stratification (M_q) can be expressed as

$$M(x, y) = \Delta p_t^{-1} \int_{p_t}^{p_0} (-\partial_p \overline{h}) \Omega(p)\, dp, \quad (2.1a)$$

$$M_q(x, y) = \Delta p_t^{-1} \int_{p_t}^{p_0} (\partial_p \overline{q}) \Omega(p)\, dp, \quad (2.1b)$$

where

$$\Omega(p, x, y) = -\int_{p}^{p_0} (A^+(\dot{p}) - \widehat{A^+})\, d\dot{p}, \quad (2.2a)$$

$$A^+(p, x, y) = \int_{p}^{p_0} A(\dot{p}, x, y)\, d \ln \dot{p}, \quad (2.2b)$$

and $A(p, x, y)$ give the vertical structure of temperature perturbations under convective QE constraints

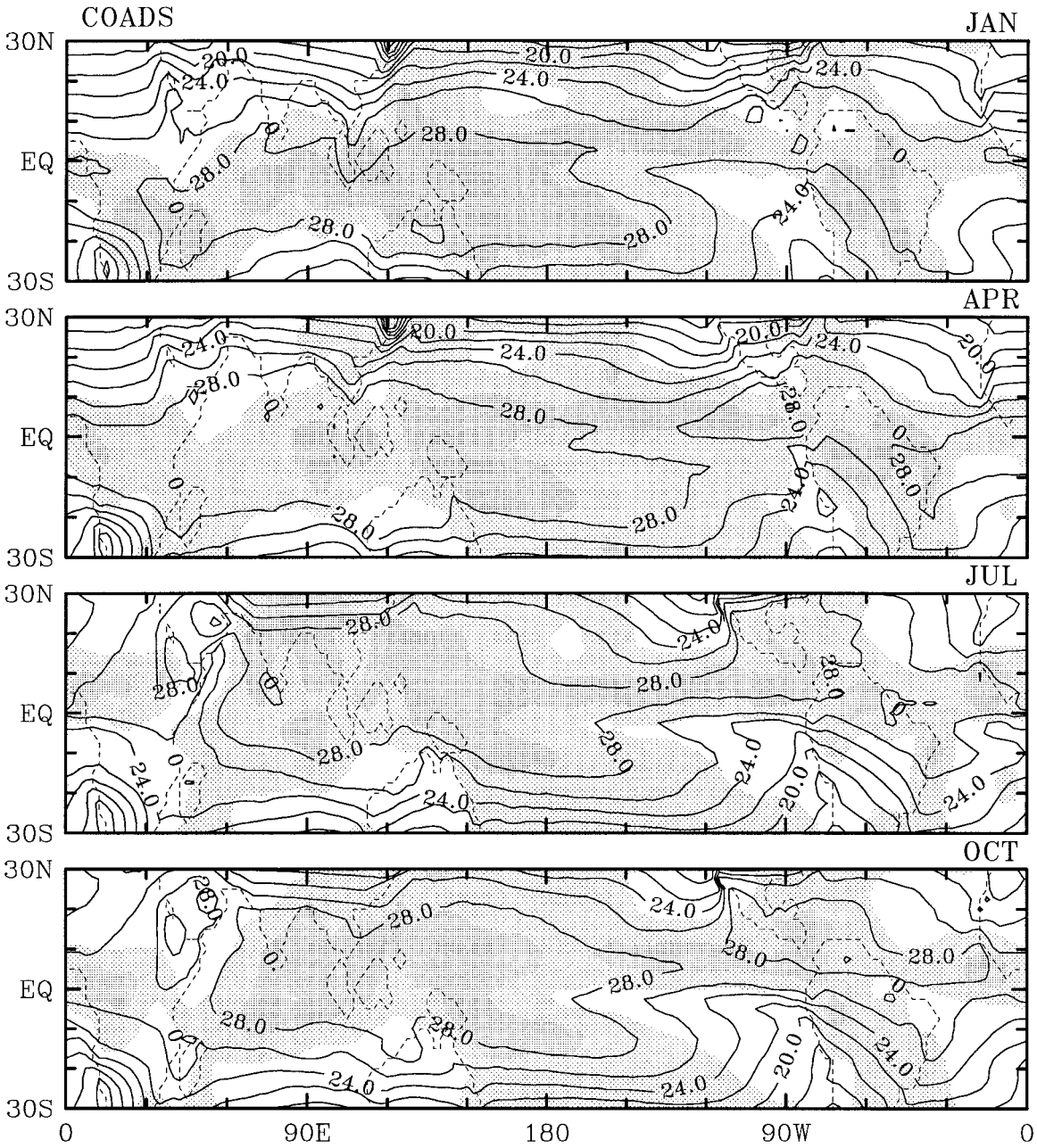

FIG. 1. Seasonal cycle of the sea surface temperature (contours) and precipitation (stippling) climatology in January, April, July, and October from the Comprehensive Ocean–Atmosphere Data Set. Heavy stippling denotes values greater than 200 mm month^{-1}, while light stippling denotes values greater than 50 mm month^{-1}.

$$T' = A(p, x, y)h_b', \tag{2.3}$$

where $h_b' = T_b' + q_b'$ is the planetary boundary layer (PBL) moist enthalpy perturbation. Overbars denote a climatological state that is assumed to be varying slowly in space such that horizontal gradients of $A(p, x, y)$ are small. Primes denote perturbations from this state. Taking A to be approximately given by the moist adiabat yields

$$A(p, x, y) = (1 + \gamma)^{-1} \exp\left[-\kappa \int_p^{p_b} (1 + \gamma)^{-1}\, d \ln p\right],$$

$$p_b \geq p \geq p_t; \tag{2.4a}$$

$$A(p, x, y) = (1 + \gamma_b)^{-1}(p/p_b)^{\kappa}, \qquad p_0 \geq p \geq p_b. \tag{2.4b}$$

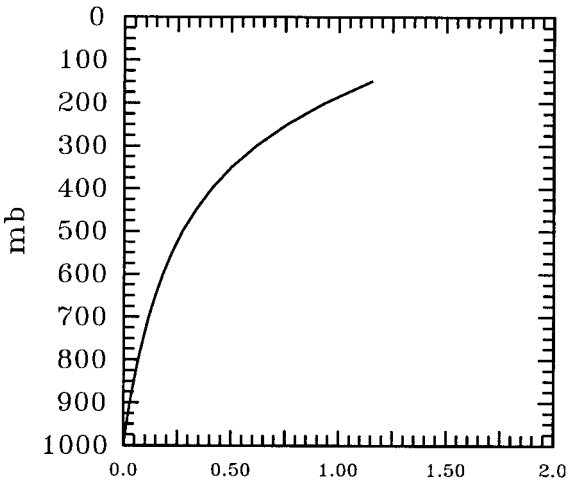

FIG. 2. Vertical profile of A^+ (which gives the vertical structure of baroclinic pressure gradients in convective regions) calculated from Jordan's (1958) profile.

Here, $\kappa = c_p/R$ measures the ratio of the specific heat at constant pressure to the gas constant; p_0 is the surface pressure, p_t the maximum depth of convection, p_b the cloud base pressure, and Δp_t the pressure depth from p_0 to p_t. The saturation mixing ratio change with respect to temperature at a given level is denoted $\gamma = (dq_{\text{sat}}/dT)_{\bar{T}}$ and γ_b is its cloud base value. We note that since QE constraints on temperature apply over the depth in which deep convection frequently occurs, the integrals are taken from the PBL to the maximum depth of convection. Also in (2.2a), we have used

$$\widehat{(\,)} = \Delta p_t^{-1} \int_{p_t}^{p_0} (\,)\, dp$$

for vertically averaged quantities.

The quantity A is the characteristic vertical structure of temperature perturbations constrained by convection to be approximately moist adiabatic. It is worth noting that the vertical change of A is typically much larger than the horizontal change. Neelin and Yu also showed that M is not very sensitive to details of the structure of A. Betts and Miller (1986) use a profile of A that differs slightly from the moist adiabat, but the approximation of using the moist adiabat in (2.4) makes little difference. The vertical profile of A^+ calculated from Jordan's (1958) sounding is shown in Fig. 2 for reference. It gives the vertical structure of baroclinic pressure gradients resulting from temperature perturbations of the form (2.3). The quantity $\Omega(p, x, y)$ is the shape of the vertical velocity profile for inviscid motions obeying these convective constraints and subject to upper and lower boundary conditions of vanishing vertical velocity. Note that $\Omega(p, x, y)$ depends only on the basic-state temperature profile and changes slowly in the horizontal if A does. The sign has been chosen such that for a typical sounding profile in the Tropics, this quantity is positive (see appendix A). In (2.1a), $\overline{h} = \overline{s} + \overline{q}$ is the basic-state moist static energy, with $\overline{s}$ and $\overline{q}$ denoting the basic-state dry static energy and specific humidity, respectively. An additional quantity, M_s, the gross dry stability, may be defined by using s instead of h in (2.1a), so that $M = M_s - M_q$. The basic state in (2.1a,b) is assumed to be slowly varying in the horizontal. Since the derivation assumes that variations about the basic state are subject to moist convective QE constraints, the definitions are relevant only in regions where deep convection occurs with sufficient frequency.

We also note that the original form of M, (2.1a), is more useful in discussing the analytical interpretation. To facilitate calculations of M and M_q, we use the following alternative forms of (2.1a,b) (after employing integration by parts) for numerical calculations:

$$M = \widehat{A^+\overline{h}} - \widehat{A^+}\,\hat{\overline{h}}, \tag{2.5a}$$

$$M_q = -\widehat{A^+\overline{q}} + \widehat{A^+}\,\hat{\overline{q}}. \tag{2.5b}$$

3. Data

Three datasets are used: the first is taken directly from rawinsonde soundings. To obtain greater spatial coverage, two datasets from operational model analyses are also used. The spatial variation of the climatology of our calculated quantities is our main interest so we are forced to use the operational analyses, despite deficiencies and caveats discussed below and in Lambert (1988) and Trenberth and Olson (1988). For the actual sounding data, we select 14 rawinsonde stations inside the domain of our interest from January 1980 to December 1989. Figure 3 shows the geographical positions of these rawinsonde stations. The different sounding regions are numbered for reference. We chose these areas for two reasons: (i) they are the only stations that provide uninterrupted sounding observations in the domain of interest for the same periods as those of ECMWF and NMC model analyses, and (ii) their area means are typical of five different regional thermodynamic characteristics over the Tropics. Area I roughly represents characteristics of the central Pacific, area II the western Pacific, area III the tropical continents, and areas IV and VI the southern Pacific and Indian Oceans, respectively. Area V represents subtropical characteristics whose position is close to the edge of the domain of applicability.

Model analysis datasets are taken from ECMWF and NMC global monthly mean analyses, respectively. For ECMWF data, the temperature, relative humidity, and geopotential height data are available on seven pressure levels: 100, 200, 300, 500, 700, 850, and 1000 mb. The latitude–longitude resolution is 2.5° by 2.5°. For NMC data, nine standard pressure levels are chosen: 50, 100, 200, 250, 300, 500, 700, 850, and 1000 mb. However, values of the specific humidity are available only in the lowest four levels. Latitude–longitude resolution is 2.5°

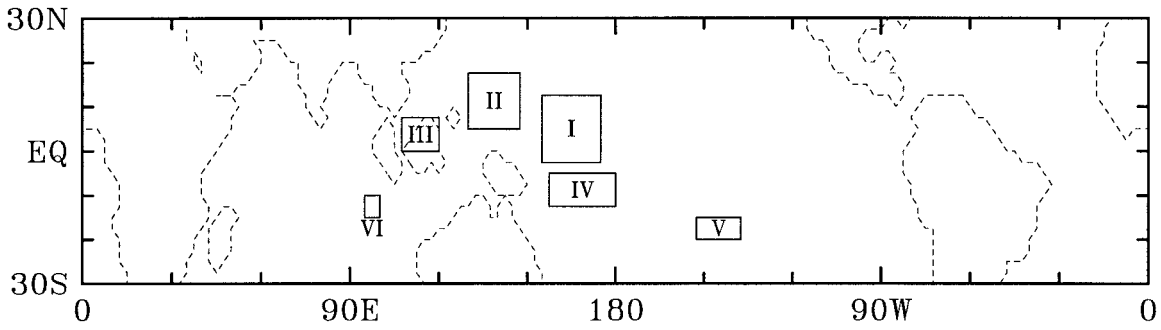

FIG. 3. The domain of selected rawinsonde stations studied in this paper. Different regions are numbered for comparison with the results from model analysis data. There are four rawinsonde stations in area I; three in area II; two in areas III, IV, and V; but only one rawinsonde station in area VI.

by 2.5°. Detailed discussion of ECMWF and NMC datasets can be found in Bengtsson et al. (1982) and McPherson et al. (1979). Prior to March 1992, the NMC dataset suffers from an error in that virtual temperature rather than temperature was recorded (J. E. Janowiak 1995, personal communication). To remedy this, we use an iterative algorithm to correct this error in deriving specific humidity and temperature. However, submonthly variations and the nonlinearity of virtual temperature imply that these corrected fields still contain some error. Thus, we use the ECMWF dataset as our primary analysis dataset and relegate the NMC dataset to a comparison in appendix B.

Since we are only interested in understanding the climatic characteristics of the gross moist stability and gross moisture stratification, a 10-yr average (from January 1980 to December 1989) of the monthly mean data is taken as the climatology.

4. Results

Since the determination of the maximum level of convection is important to the estimate of M, we first show the horizontal distribution of an estimate of this level in Fig. 4. Realistically, determining the level to which convection can extend from a given sounding is a complicated issue that could be affected by entrainment processes, etc. We simply use the level at which the moist adiabat rising from the top of PBL loses buoyancy, approximately:

$$\overline{h}(p_t) = \overline{h}_b, \tag{4.1}$$

where $\overline{h}(p_t)$ and $\overline{h}_b$ are the mean moist static energy at convective top and the PBL (characterized by 1000 mb) respectively. This estimate of the maximum level of convection is affected by the approximation $h_{\text{sat}}(p_t) \approx \overline{h}(p_t)$, by interpolation, and by the assumption of a nonentraining, pseudoadiabatic path for the highest rising convective parcels. It is biased on the high side, with the effect being small in deep convective regions but substantial in regions where the estimated level descends lower. Using $\overline{h}$, not h_{sat}, in (4.1) provides a reliable algorithm, but in regions where this level is low, the sounding may not be convectively unstable through this depth. We ignore regions with maximum level of convection at heights less than 300 mb and allow for effects of changes in the vertical extent of convection, providing a more precise estimate of the gross moist stability compared to that of Neelin and Held (1987).

Figure 4 shows the seasonal cycle of the distribution of the maximum level of convection estimated from the ECMWF climatology. Consistent with the precipitation pattern, the maximum level of convection follows the migration of SST with deeper clouds occurring over warmer ocean. In all seasons, there is an obvious boundary with strong gradients of the maximum level of convection; we take regions with the estimated climatological maximum level of convection at heights greater than 300 mb as one criterion in defining the domain of applicability of our calculation.

a. ECMWF–rawinsonde comparisons

Figure 5 compares the ECMWF gridded soundings with the actual rawinsonde profiles for the six areas delineated in Fig. 3. Here we show moist static energy (h) profiles instead of equivalent potential temperature (θ_e) profiles for consistency. Although small discrepancies can be observed, the ECMWF profiles are qualitatively similar to the actual rawinsonde profiles in most areas except in area III. There, the ECMWF data yields larger values of h and h_{sat} in the entire troposphere, and the difference is larger in the lower troposphere than in the middle and upper troposphere due to significant low-level moisture and temperature errors in the ECMWF data.

Table 1 lists the values of M, M_q, and p_T estimated from rawinsonde and ECMWF data. The standard deviations between individual stations within each area are given as a measure of how sensitive these qualities are to small differences between soundings. There is rough agreement between rawinsonde and ECMWF values, but substantial systematic errors are found, despite

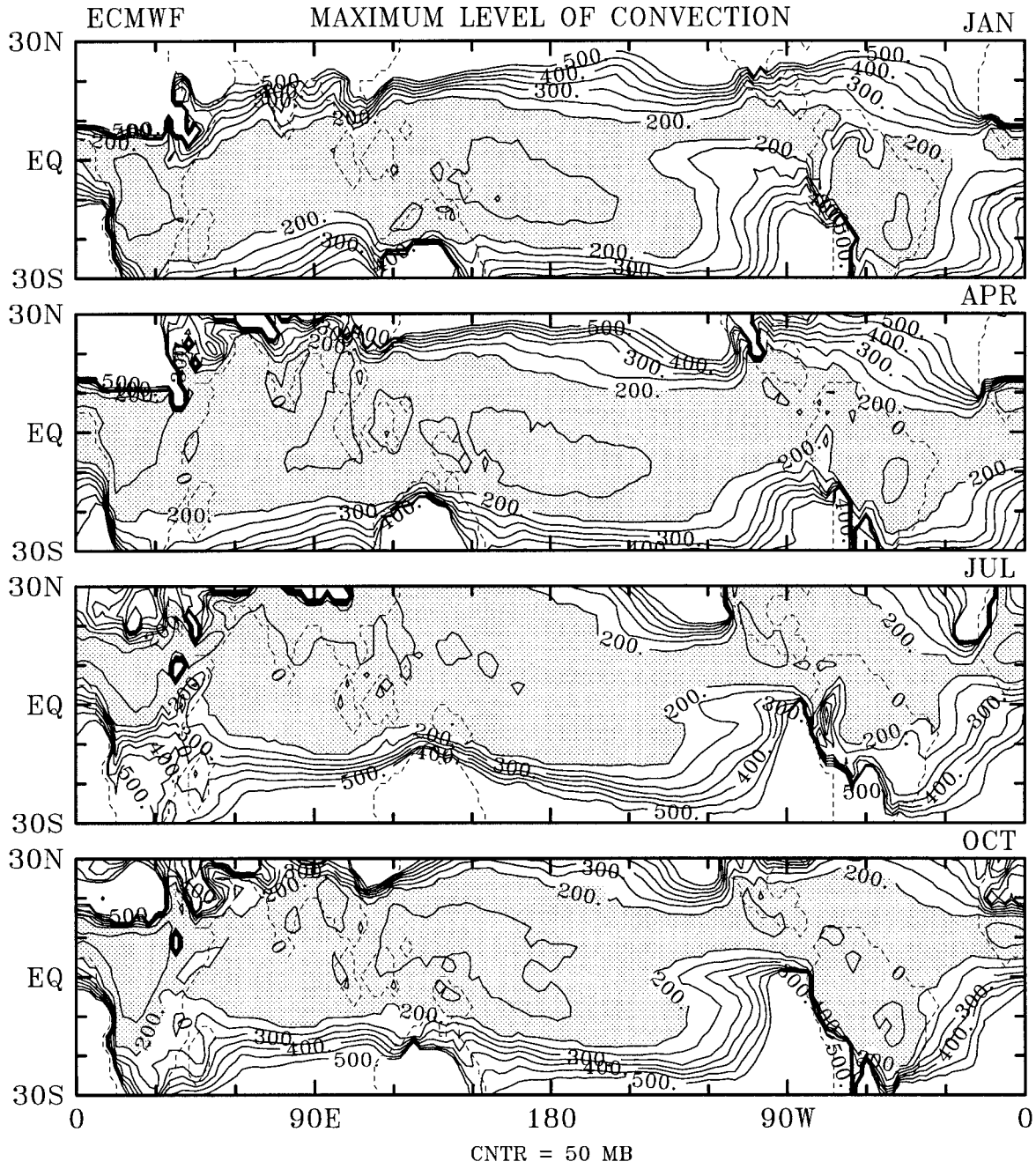

FIG. 4. Seasonal cycle of the maximum level of convection distribution estimated from ECMWF climatology in January, April, July, and October. The maximum level of convection is defined as the highest possible cloud top estimated using (4.1). Contour interval 50 mb; stippled over 200 mb.

the apparent closeness of the profiles between rawinsonde and ECMWF soundings. Except in region VI, ECMWF soundings underestimate values of M because higher h in the upper troposphere gives a lower maximum level of convection. Errors in M are smaller than if errors in M_q and M_s were independent. This is because a strong cancellation between high surface moisture values (giving large M_q) and higher p_T (giving larger M_s) results in smaller M errors. Since the *square root* of M characterizes the propagation speed of the waves obeying QE constraints (see appendix A), errors in phase speed will be smaller than errors in M. The comparison here suggests that the ECMWF data can provide a qualitative picture of the distribution of M and M_q over tropical oceans, although quantitative aspects should be interpreted with caution.

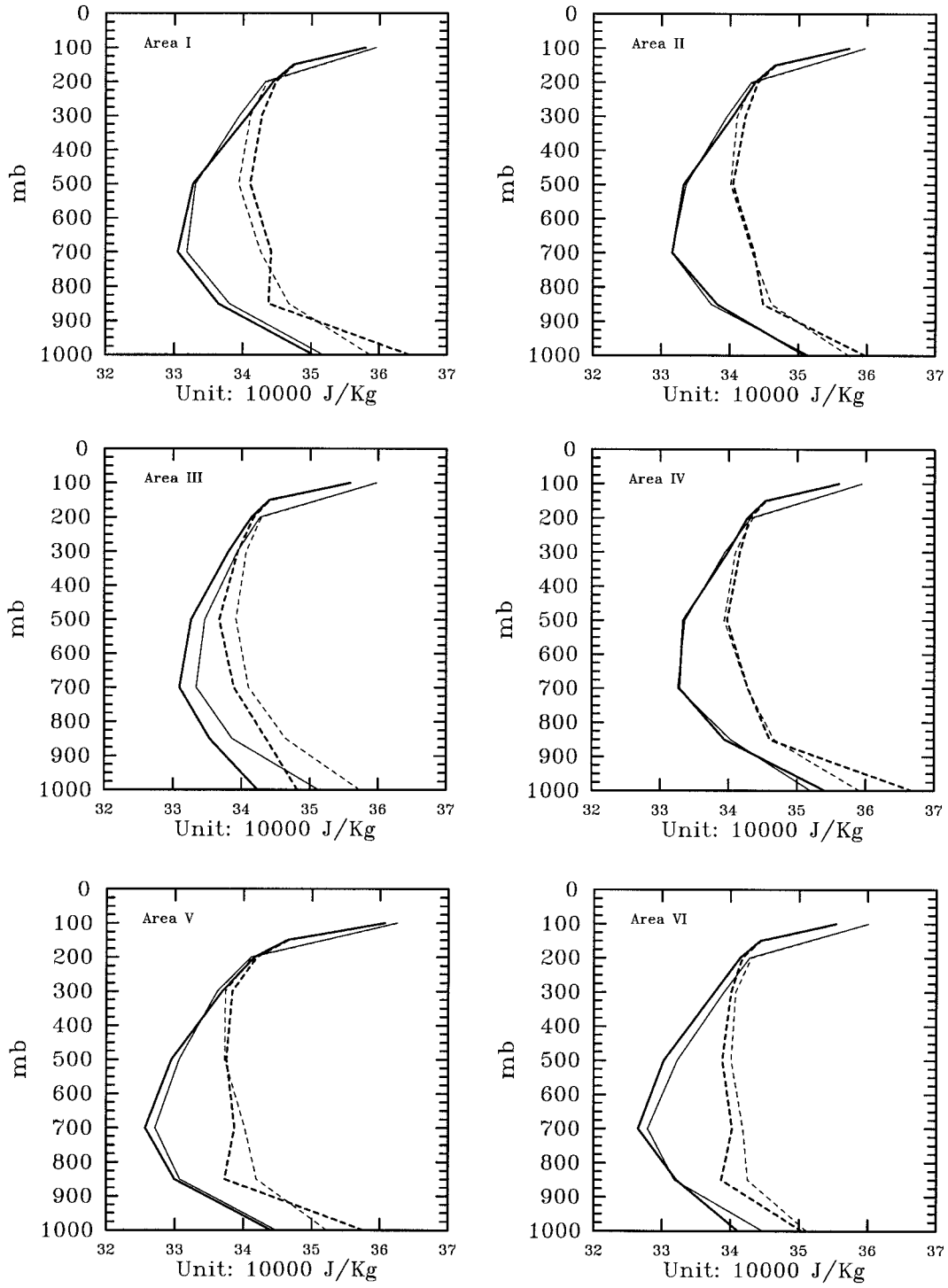

FIG. 5. A comparison between the rawinsonde soundings (heavy lines) and ECMWF analyses (light lines) in the six regions defined in Fig. 3. The solid lines are moist static energy ($\overline{h}$) profiles and the dashed lines denote saturation moist static energy ($\overline{h}_{sat}$) profiles. An annual average for the period from January 1980 to December 1989 is taken.

b. Gross moist stability

Figure 6 presents the seasonal cycle of the gross moist stability (M) distribution estimated from ECMWF data. Cross-hatched lines denote regions outside the domain of applicability. We have used a criterion that mean precipitation should be greater than 50 mm month^{-1} and maximum level of convection should be less than 300 mb for the domain of applicability, indicating regions with substantial amounts of deep convection. These values are chosen as rough indicators, based on typical climatological values of precipitation and deep convective top, and are not sharp definitions of the region of validity. In Fig. 6, the sudden decrease in M near the edge of the domain of applicability is a further indicator of where assumptions fail. Within the domain of applicability, we do observe smaller values of M in the central and western Pacific regions where SST is warmer. Overall, the change of M is modest. Its values range from 200 J kg^{-1} in the central and western Pacific to 800 J kg^{-1} in the subtropical Pacific, corresponding to a phase speed change from 8 to 16 m s^{-1} as implied by (A4). Most of the region remains near 500 J Kg^{-1}.

Compared to the gross moist stability defined in the two-layer model of Neelin and Held (1987), our calculation concurs that there is a well-defined gross moist stability that is much less than the dry static stability. However, the results differ in that the pattern of M is not closely linked to SST. If anything, we would characterize the M distribution as being surprisingly constant (within the domain of applicability and within the errors of the analysis dataset). The reason for this is a compensation between effects of the maximum level of convection and of low-level moisture. In regions of high surface moisture (typically associated with high SST), convection extends higher, and the net moist stability remains about the same. The mechanism by which cloud-top effects modify these of low-level moisture variations is quantified at length in section 5.

c. Gross moisture stratification

Figure 7 displays the seasonal cycle of the gross moisture stratification (M_q) distribution as estimated from the ECMWF data. In contrast to the gross moist stability, the pattern of M_q is strongly influenced by the ocean surface conditions such that it closely follows the SST distribution, with larger values of M_q occurring over warmer ocean. Significant zonal and meridional gradients of M_q are found for all seasons, even in the convergence zones. The magnitude ranges from 1500 to 3500 J kg^{-1} in the domain of interest. The 2500 J kg^{-1} contour lines roughly coincide with the 28°C SST isotherms and 1500 J kg^{-1} contours with the 24°C SST isotherms. Since most moisture is confined to the lower troposphere and is significantly governed by its saturation value, this strong link between SST and M_q is expected.

There is also strong resemblance between the M_q distribution and the climatological precipitation pattern. Except for the eastern Pacific convergence zone, the 2500 J kg^{-1} contour lines in Fig. 7 roughly coincide with the the edge of 200 mm month^{-1} in Fig. 1. Since M_q measures the moisture available for precipitation in presence of large-scale convergence, the results presented in Fig. 7 quantify the spatial inhomogeneity of the moisture reservoir in the tropical atmosphere. That is, given the same convergence perturbation, the precipitation response will be greater in the western Pacific compared to that in the eastern Pacific simply due to inhomogeneous M_q. In this regard, the present results concur with the earlier Neelin–Held version.

5. Further analyses of M

To understand competing effects causing M not to vary strongly despite large changes in moisture, we consider the effects on M of a general modification to the moist static energy profile, using (2.1a). To facilitate discussion, we separate the gross moist stability into a horizontal mean component and a component due to departures from this

$$M = \langle M \rangle + M^*, \tag{5.1}$$

where $\langle M \rangle$ is the gross moist stability horizontally averaged over the entire domain of interest and M^* denotes departure from the horizontal mean. The same analysis would apply with angle brackets denoting a more general reference state and asterisks denoting any modification. The modification of the gross moist stability M^* can further be divided into components associated with departures of moist static energy h^* and with departures of cloud-top p_t^*:

$$M^* = M^*_{\overline{h}} + M^*_{p_t}, \tag{5.2a}$$

where

$$M^*_{\overline{h}} = \langle \Delta p_t \rangle^{-1} \int_{\langle p_t \rangle}^{p_0} (-\partial_p \overline{h}^*) \langle \Omega(p) \rangle \, dp, \tag{5.2b}$$

$$M^*_{p_t} = M - \langle M \rangle - M^*_{\overline{h}} \tag{5.2c}$$

$$= \langle \Delta p_t \rangle^{-1} \left[\int_{\langle p_t \rangle - p_t^*}^{\langle p_t \rangle} (-\partial_p \langle \overline{h} \rangle) \Omega(p) \, dp - \int_{\langle p_t \rangle}^{p_0} (\partial_p \langle \overline{h} \rangle) \Omega^*(p) \, dp \right] + O(h^* p_t^*), \tag{5.2d}$$

and where $\Omega^*(p)$ gives departure in $\Omega(p)$ from the case with unperturbed cloud top.

The term $M^*_{\overline{h}}$ represents departures solely due to variations of $\overline{h}$. Since $\langle \Omega(p) \rangle$ is always positive within the column $p_0 \geq p \geq \langle p_t \rangle$, the sign of $M^*_{\overline{h}}$ thus depends only on the vertical profile of $\partial_p \overline{h}^*$. The term $M^*_{p_t}$ is defined in (5.2c) as a residual due to cloud-top variations

TABLE 1. Estimates of the gross moist stability M and the gross moisture stratification M_q calculated from monthly mean rawinsonde climatology and ECMWF data. Also shown are the gross dry stability M_s and the maximum level of convection p_T. Values of standard deviation within each area are shown with ± signs. The domain of the selected areas is shown in Fig. 3.

Area	Data source	M	M_q	M_s	p_T
I	Rawinsonde	700 ± 23	3220 ± 45	3920 ± 154	120 ± 9
	ECMWF	490 ± 10	2870 ± 136	3360 ± 105	160 ± 5
II	Rawinsonde	660 ± 9	3110 ± 210	3780 ± 178	130 ± 8
	ECMWF	520 ± 16	2800 ± 108	3320 ± 66	160 ± 3
III	Rawinsonde	420 ± 9	2830 ± 164	3250 ± 196	160 ± 12
	ECMWF	350 ± 14	2970 ± 136	3360 ± 164	160 ± 8
IV	Rawinsonde	590 ± 7	3360 ± 273	3990 ± 297	120 ± 12
	ECMWF	380 ± 13	3010 ± 178	3390 ± 224	150 ± 11
V	Rawinsonde	800 ± 8	2590 ± 91	3390 ± 119	160 ± 7
	ECMWF	520 ± 12	2200 ± 52	2730 ± 10	190 ± 0
VI	Rawinsonde	520	2270	2800	200
	ECMWF	590	2130	2760	200

for simplicity of calculation. If $p_t^* = 0$, then $M_{p_t}^* = 0$ by definition. For positive p_t^*, the first and second terms on the right-hand side of (5.2d) are positive. In other words, if cloud top becomes higher, the correction of M due to cloud-top effect is positive.

a. Simplified examples

To discuss variations of M due to $\overline{h}$ and p_T changes, two idealized cases are chosen. To avoid dealing with the variation of A^+ with temperature, we consider that the variation of $\overline{h}$ is mainly due to moisture. First, we consider a case with a modification that affects the PBL, and thus also affects cloud-top level, as shown in Fig. 8. Let the moisture increase q^* be

$$q^* = \eta_1(p) q_b^*, \tag{5.3a}$$

where q_b^* is the maximum moisture departure in the PBL and η_1 is a linear function of pressure given by

$$\eta_1(p) = \begin{cases} 0, & p_m > p \\ (p - p_m)/(p_b - p_m), & p_b > p \geq p_m \\ 1, & p \geq p_b. \end{cases} \tag{5.3b}$$

Using (5.3a), (5.3b) in (2.1a) and (5.2) yields the following corrections to the gross moist stability due to low-level moisture increase and cloud-top variation, respectively:

$$M_{\overline{h}}^* = -[\langle \Delta p_t \rangle (p_b - p_m)]^{-1} q_b^* \int_{p_m}^{p_b} \langle \Omega(p) \rangle \, dp, \tag{5.4a}$$

$$M_{p_t}^* = (\langle \Delta p_t \rangle \, p_t^*)^{-1} q_b^* \int_{\langle p_t \rangle - p_t^*}^{\langle p_t \rangle} \Omega(p) \, dp + (p_t^*/\langle \Delta p_t \rangle) A^+(\langle p_t \rangle)[\langle \overline{h}(\langle p_t \rangle) \rangle - \langle \hat{\overline{h}} \rangle]. \tag{5.4b}$$

Here, we have used the approximation, $\partial_p \overline{h}|_{\langle p_t \rangle} \approx -q_b^*/p_t^*$ in deriving (5.4). For this case (Fig. 8), $M_{\overline{h}}^*$ in (5.4a) is negative while $\Delta M_{p_t}^*$ is positive. That is, the low-level moisture increase tends to lower the value of M but the cloud-top effect tends to increase it. Both effects are of equal importance in modifying the value of M. Since the cloud top and the low-level moisture changes are intimately related and strongly cancel each other, M changes only modestly with q_b^*. It is also worth noting that $M_{\overline{h}}^*$ approaches a finite value as $p_m \to p_b$, so this formula gives qualitatively similar results whether the moisture increase is restricted entirely to the PBL or drops off more slowly with height.

We next assume a lower midlevel modification of the moisture profile, as shown in Fig. 9, without affecting the PBL (and thus cloud top). The moisture departure q^* is assumed to be

$$q^* = \eta_2(p) q_{\max}^*, \tag{5.5a}$$

where $q_{\max}^*$ is the maximum departure at level $p = p_m$, and $\eta_2(p)$ is given by

$$\eta_2(p) = \begin{cases} 0, & p_u > p \\ (p - p_u)/(p_m - p_u), & p_m > p \geq p_u \\ (p_b - p)/(p_b - p_m), & p_b > p \geq p_m \\ 0, & p \geq p_b, \end{cases} \tag{5.5b}$$

so the moisture change is confined in the lower midlevels.

The moisture change given by (5.5a), (5.5b) yields a correction to the gross moist stability:

$$M_{\overline{h}}^* = \langle \Delta p_t \rangle^{-1} \left[(p_b - p_m)^{-1} \int_{p_m}^{p_b} \langle \Omega(p) \rangle \, dp - (p_m - p_u)^{-1} \int_{p_u}^{p_m} \langle \Omega(p) \rangle \, dp \right] q_{\max}^*. \tag{5.6}$$

Here $M_{p_t}^* = 0$ because no cloud-top variation occurs in this case. It is noted that the two terms on the right-hand side of (5.6) are opposite in sign, giving cancellation in M^* in this case as well. For instance, for the

case of an idealized profile of $\Omega(p)$ as a quadratic with maximum absolute value $\Omega_{\max}$ at level p_ω,

$$\Omega(p) = \begin{cases} \Omega_{\max}\{1 - [(p - p_w)/(p_t - p_w)]^2\}, \\ \quad p_\omega > p \\ \Omega_{\max}\{1 - [(p - p_w)/(p_b - p_w)]^2\}, \\ \quad p \geq p_\omega. \end{cases} \tag{5.7}$$

We find that $M_h^* = 0$ when $p_u = p_t$ and $p_m = p_\omega$. This does not hold exactly in general but, as a rule of thumb, M_h^* has opposite sign to the moisture change when the maximum absolute value of the moisture departure occurs at levels lower than $\Omega_{\max}$. This is the case for typical moisture variations since at upper levels variation of q is small.

b. Two-dimensional analysis using ECMWF analysis data

We now use (5.2a) to examine quantitatively the two competing effects, low-level moisture increase and cloud-top change, in modifying the gross moist stability as a function of space in the climatology. The term M_h^* in (5.2b) is due to variation of moist static energy stratification (integrated in the vertical) in fixed cloud-top calculations. The term $M_{p_t}^*$ in (5.2c) is primarily due to cloud-top change. Both mid- and low-level h variations affect M_h^* while PBL h variations dominate $M_{p_t}^*$, as discussed in section 5a. Neglecting the term $M_{p_t}^*$ in (5.2a) can yield similar results (not shown) to the two-level model of Neelin and Held (1987).

Figure 10 shows longitude–latitude sections of the gross moist stability variations (defined as the deviation from horizontal mean) in the tropical Pacific due to M_h^* (Fig. 10a) and $M_{p_t}^*$ (Fig. 10b) calculated from ECMWF annual mean climatology. Here, $\langle M \rangle$ is estimated to be about 420 J kg^{-1}. In the central and western Pacific convergence zones, M_h^* is negative (by as much as 600 J kg^{-1}) due to warmer SST and greater low-level moisture in these regions. The cloud-top effect $M_{p_t}^*$ provides positive corrections in the central and western Pacific convergence zones that nearly cancel M_h^*. Figure 10c shows the combination of both effects, with dramatically reduced variations (less than 200 J kg^{-1} in most areas) and little relation to SST. Except in the western equatorial Pacific, the correction due to cloud-top effect is typically slightly larger than that due to M_h^*. A caveat is that the maximum level of convection is used and our estimate of this is biased high, so we may be overestimating the p_t^* effect.

6. Implications

a. Madden–Julian oscillation

1) PHASE SPEED

One of the main physical consequences of the gross moist stability is its effect on the phase speed of atmospheric motions in deep convective regions. The most notable of such wave phenomena is the MJO. We refer to the moist mode with Kelvin wave meridional structure in the NY model as the MJ mode. If one neglects the viscosity due to mechanical and thermal effects, the slow phase speed of the MJ mode is approximated by (see NY)

$$C \approx [MR/(C_p A^*)]^{1/2}, \tag{6.1}$$

where M is the gross moist stability defined in (2.1) and $A^* = \hat{A} + \widehat{\alpha\gamma A}$ [see (A.7)]; $C_p A^*$ is a quantity denoting thermal inertia associated with the large-scale QE motions with $A^* = \hat{A} + \widehat{\alpha\gamma A}$ [see (A.7)]. Since we have shown that M changes only modestly within the deep convection region, the effect of A^* on phase speed of the MJ mode becomes of interest. Figure 11 shows the horizontal distribution of A^* calculated from annual mean ECMWF climatology with $\alpha = 1.0$. We note that the A^* distribution is almost homogeneous in the convergence zones. A detailed investigation (not shown) by separating A^* into temperature contribution, $\hat{A}$, and moisture contribution, $\widehat{\alpha\gamma A}$, indicates that a strong cancellation between these two terms results in a homogeneous distribution of A^* in deep convection regions. This implies that the phase speed change of the MJ mode due to inhomogeneous basic state is also modest so long as the mode remains in deep convective regions, and considering divergence, wind, or temperature as the quantities used to measure phase speed. As discussed in the next section, precipitation can behave differently. The square-root dependence of phase speed also tends to reduce variations with M and A^*.

2) PRECIPITATION

From Yu and Neelin (1997), we note that the strength of precipitation does not depend solely on the strength of convergence but is also dictated by the magnitude of M_q. To illustrate, we impose a steady divergence pattern of the baroclinic wind, $\mathbf{V}_T'$, as a forcing with a constant phase speed moving across the tropical Pacific. The idealized divergence pattern is given by

$$\nabla \cdot \mathbf{V}_T' = D_{\max} \exp[-y^2/(2L_y^2)] \sin[(x - ct)2\pi/L_x] \tag{6.2}$$

over one half-wavelength of the sinusoid, where $L_x = 180°$ is the zonal wavelength of the forcing, $L_y = 6°$ is the decay scale away from the equator, $D_{\max} = 2 \times 10^{-5}$ s^{-1} in (6.2) denotes the maximum amplitude of the prescribed divergence field, and c is the phase speed mimicking MJO-like propagation.

Figure 12 displays the precipitation response [calculated from (A8)] in five different phases to mimic a constant eastward-moving convergence field associated with the Kelvin-wave-like MJO. These five different phases correspond to five convergence forcing centers at 90°E, 135°E, 180°, 135°W, and 90°W. Two prominent features are found. First, the atmosphere

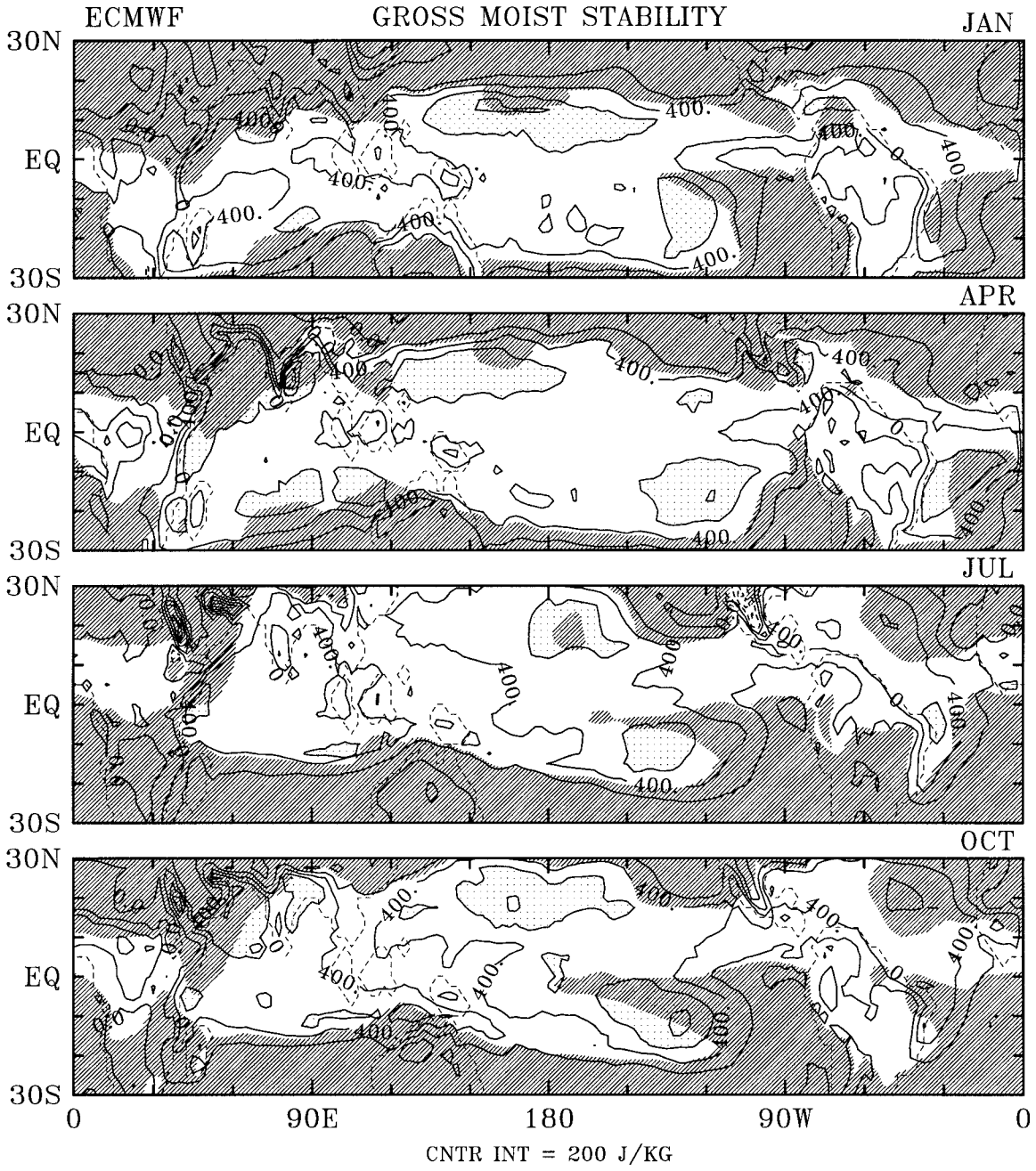

FIG. 6. Seasonal cycle of the gross moist stability (M) distribution estimated from ECMWF climatology in January, April, July, and October. Regions outside the domain of applicability (see text) are crosshatched. Contour interval 200 J kg^{-1}; stippled over 600 J kg^{-1}.

exhibits a quite different precipitation response in each phase due to differences in the moisture reservoir (M_q). A stronger precipitation response is found when the forcing is applied in the central and western Pacific, a relatively weaker response appears in the eastern Pacific, and a rejuvenation is found in the vicinity of South America. Second, the propagation of the precipitation pattern is significantly retarded in the central and western Pacific regions. From phase 1 to phase 4, the convergence center travels 135° of longitude while the precipitation center travels only about 95° of longitude. The convergence pattern has a given phase speed of 15 m s^{-1}, while the precipitation pattern appears to have a propagation speed of about 11 m s^{-1} from phase 1 to phase 4. The results presented here indicate that it can be misleading if one only utilizes the deep convection signal (e.g., the outgoing longwave radiation in observations or pre-

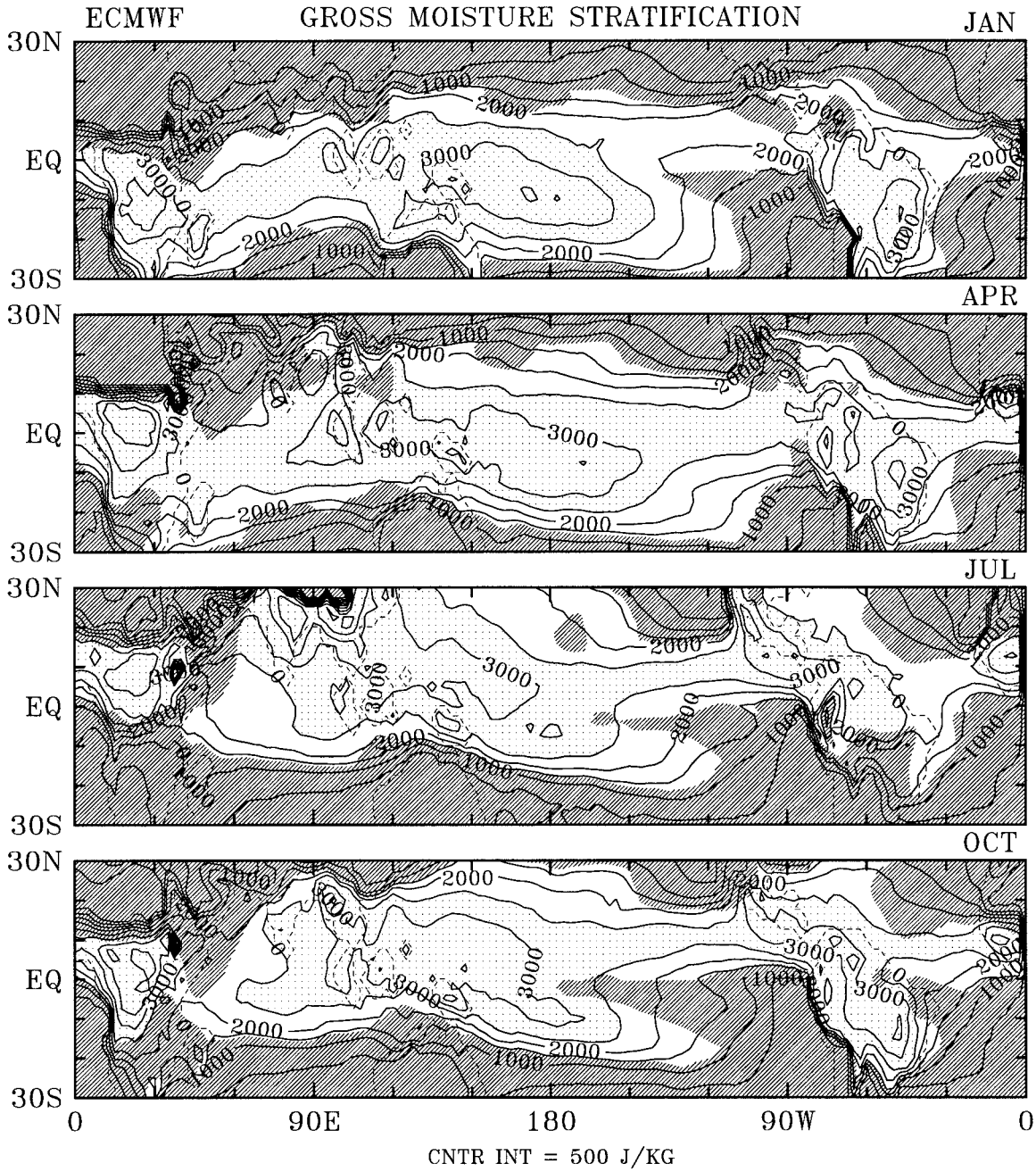

FIG. 7. As in Fig. 6 except for the gross moisture stratification (M_q) distribution. Contour interval 500 J kg^{-1}; stippled over 2500 J kg^{-1}.

cipitation in models) as a measure of the MJO propagation.

b. Gill-like models

That magnitudes of the gross moist stability distribution are less sensitive to the SST distribution compared to the gross moisture stratification explains why simple Gill-like models (e.g., Gill 1980; Zebiak 1982, 1986; Weare 1986; Lindzen and Nigam 1987; and many others) can obtain plausible results while using constant phase speeds for simulating winds. The propagation tendency of the equatorially trapped waves, which is dictated by the gross moist stability (NY; Yu and Neelin 1997), is relatively ''flat'' in our estimates. This implies that the overall stratification felt by motions in deep convective regions is not too far from the simple model approximation of constant phase speed, so far as the

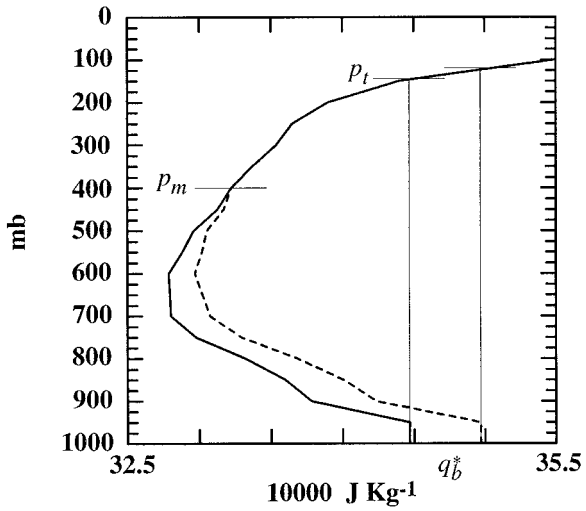

FIG. 8. An idealized case to illustrate effects of low-level moisture changes on the gross moist stability. The Jordan (1958) moist static energy profile (solid line) is perturbed with added moisture (dashed line). The maximum moisture perturbation, q_b^*, occurs in the boundary layer. The associated change in the maximum level of convection (as calculated by raising a parcel from the boundary layer with constant h) is also indicated.

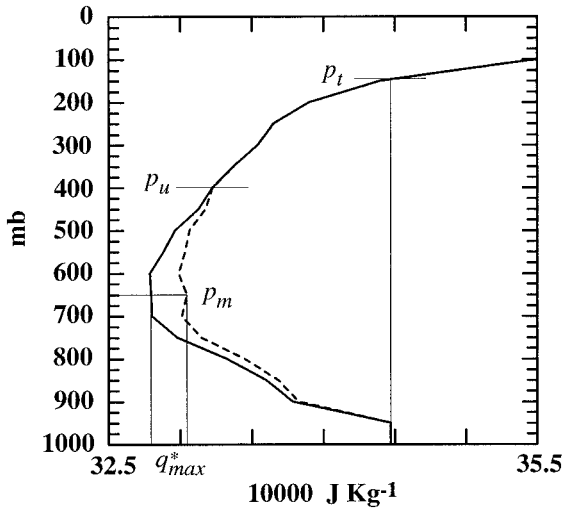

FIG. 9. As in Fig. 8 except for a midlevel moisture perturbation. The maximum perturbation of moisture, q^*_{max}, occurs at 650 mb, while the boundary layer moisture is unaffected.

dynamical response is considered. This may partially explain why these simple models all have some degree of success in ENSO studies despite simple physical assumptions. Ironically, models that use a convergence-feedback parameterization with varying lower-layer moisture but fixed vertical structure of the heating may actually do worse than simple models that use a constant moist stratification assumption. As shown in section 5, changes in the depth of convection can substantially compensate for increases in low-level moisture.

The precipitation (or heating) response, however, may be very different from the Gill-like models due to inhomogeneous moisture reservoir in the tropical atmosphere. In the Yu and Neelin (1997) model, aside from the low-level convergence, the precipitation also depends on the gross moisture stratification. Because the gross moisture stratification is strongly affected by the ocean surface conditions, the precipitation response per unit of low-level convergence tends to be stronger in the western Pacific than that in the eastern Pacific due to inhomogeneous M_q. However, the larger precipitation response does not directly affect the response of the dynamics to SST, which is dictated by M.

7. Conclusions

In this paper, we present a quantitative examination of the spatial distribution of the gross moist stability and gross moisture stratification using 10-yr monthly mean datasets from rawinsonde sounding and model analyses from ECMWF and NMC. Our results show that, in contrast to traditional intuition about the net stability of the tropical atmosphere, the gross moist stability (M) is affected by ocean surface conditions (notably the SST) in a subtle way. In the convergence zones, its magnitude varies modestly from 200 to 800 J kg^{-1}, corresponding only to a phase speed change from 8 to 16 m s^{-1}. Further analyses indicate that significant cancellation between the cloud-top effect (which acts to increase the value of M by redistribution of the moist static energy through a deeper column) and the low-level moisture change (which acts to decrease the value of M by increasing the moist enthalpy in the boundary layer) tends to keep variations of M small in deep convection regions. We note that the results accord with the Neelin–Held (1987) theory in that the gross moist stability is small compared to typical dry static stability but is positive. However, the way that we allow the cloud-top level to vary according to the boundary layer conditions significantly modifies the Neelin–Held theory. In particular, the gross moist stability distribution does not follow SST changes in a simple fashion. Rather, the value of M changes only modestly with respect to SST distribution in deep convection regions. In the steady-state problem, the balance between the convergence–divergence of moist static energy governed by M and the net heat fluxes into the column determines the low-level convergence. In carrying out such calculations, care must be taken to include the vertical structure of the wind field given by (A.5).

The pattern of gross moisture stratification (M_q), on the other hand, is strongly regulated by the SST with significant horizontal gradient observed in the domain of interest. Larger values of its magnitude tend to occur over warmer SST areas. The pattern also marks the positions of convergence zones with the 2500 J kg^{-1} contours roughly coinciding with the 200 mm mo^{-1} contours. It is noted that a simple correspondence between the magnitude of gross moisture stratification and SST

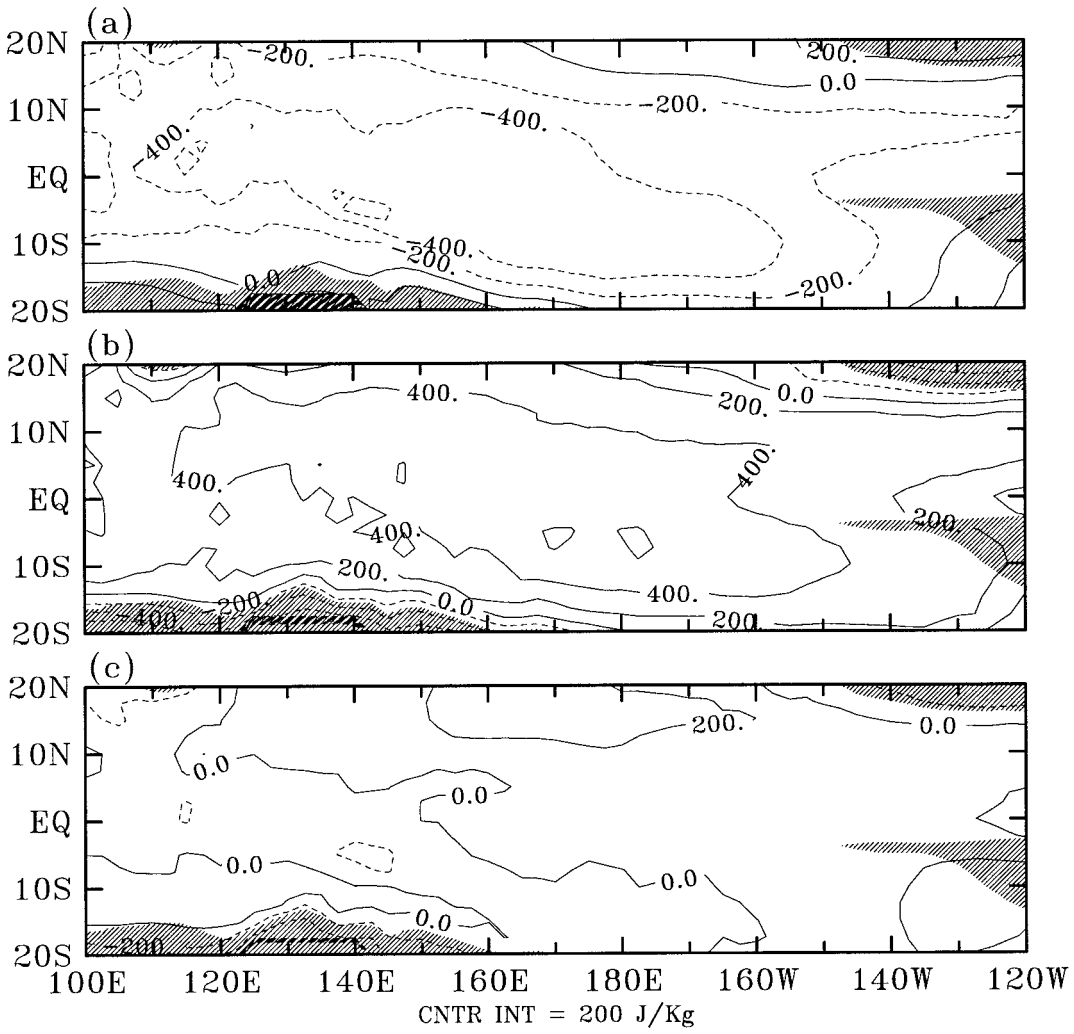

FIG. 10. Longitude–latitude (Pacific region) maps of the gross moist stability departures from the horizontal mean estimated from ECMWF annual mean climatology (a) due to variations of $\partial_p h$ [i.e., M_h^* in (5.2b)], (b) due to cloud-top effect [i.e., $M_{p_t}^*$ in (5.2c)], and (c) the combination of the above two effects. Contour interval 200 J kg^{-1}; crosshatched outside the domain of applicability.

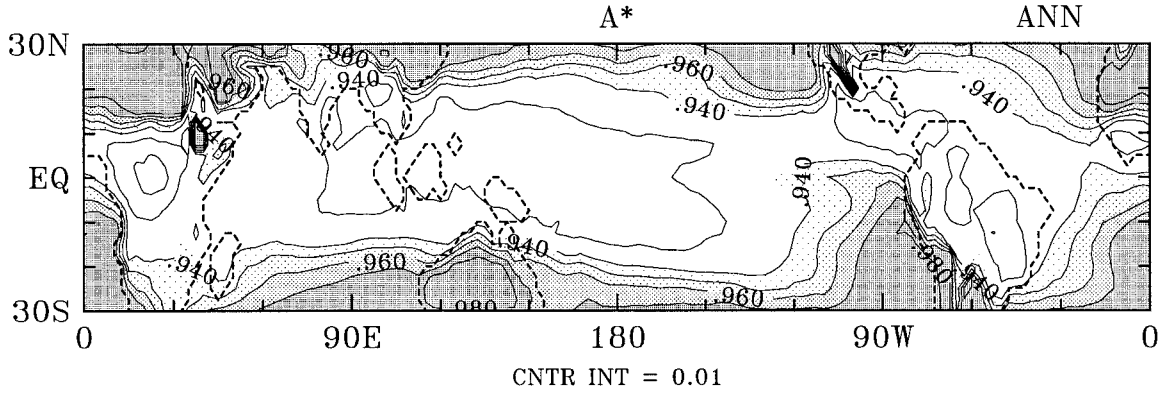

FIG. 11. Horizontal distribution of the thermal inertial quantity, A^*, calculated from annual mean ECMWF climatology. Contour interval 0.01 (nondimensional).

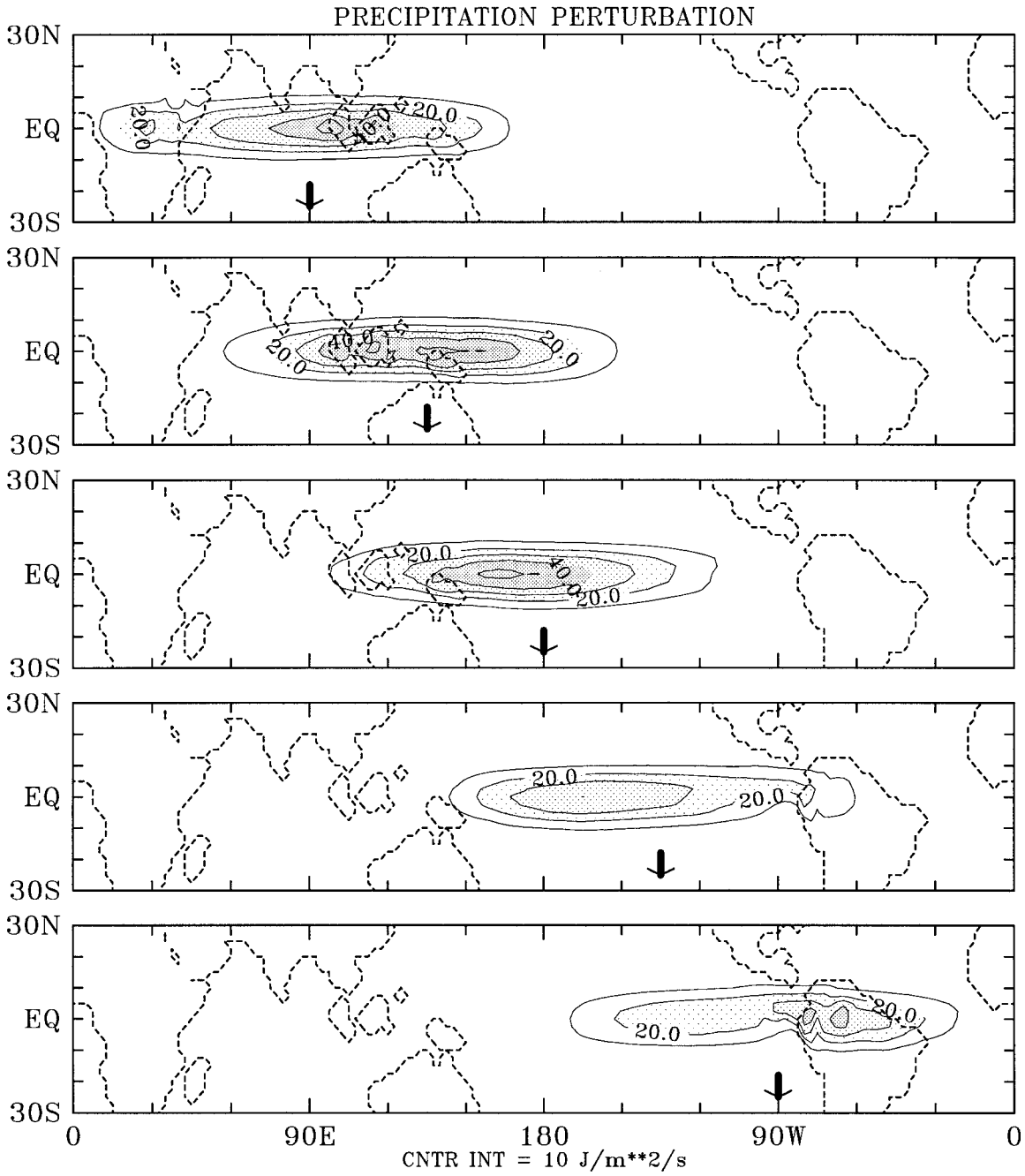

FIG. 12. The precipitation response in five phases of an idealized Madden–Julian oscillation-like convergence field (6.2) propagating at constant phase speed along the equator. These five phases, from top to bottom, correspond to the response when forcing centers (denoted by heavy arrows) are placed at 90°E, 135°E, 180°, 135°W, and 90°W, respectively.

is evident regardless of cloud-top effects. Since M_q provides a measure of the basic-state moisture available for precipitation, its horizontal variations summarize the inhomogeneity of the moisture reservoir. This implies that the western Pacific should have a stronger precipitation (or heating) response per unit convergence compared to the eastern Pacific. However, this stronger precipitation response is not linked to a reduction in the effective stratification felt by the large-scale rising motions since the heating is distributed over a deeper layer. Thus, simple Gill-like models that use a constant moist phase speed may actually do better, in dynamical aspects, than models that have a fixed-depth heating proportional to convergence. The analysis here points to considerable importance of changes in the depth of heating in compensating for low-level moisture variations.

The use of M and M_q in interpreting the slowly varying large-scale phenomena applies in deep convection regions. The domain of applicability of this study is restricted to regions in which deep convection occurs often enough to constrain large-scale temperature fields. Extension of the theory used here to nondeep-convective regions, such as the subtropics and parts of the eastern Pacific, is the subject of ongoing work as outlined in Neelin (1997). Essentially, the effective stability switches from M in convective regions to the much larger dry static stability in nonconvective regions. Within the deep convective regions, one of the most useful results for thinking about the large-scale flow is simply that M is positive and not highly variable. This implies that it does make sense to consider a stable large-scale response of the tropical atmosphere to forcing by lower boundary conditions, even when cloud-scale motions are unstable.

Acknowledgments. This work was supported under NSF Grant ATM-9521389 and NOAA Grant NA46GP0244. The first author was also partially supported by the National Sciences Council in Taiwan under Grant NSC85-2111-M-034-002. ECMWF, NMC, and rawinsonde data were provided by the Data Support Section at the National Center for Atmospheric Research.

APPENDIX A

Analytic Approximations for Moist Convective Regions

This paper is motivated by analytic approximations for moist convective regions under quasi-equilibrium convective constraints originated by Neelin and Yu (1994) and elaborated upon by Yu and Neelin (1997). Major simplifications of the tropical dynamics come directly from the QE assumptions employed by the Betts–Miller (1986) parameterization of convective heating. The QE assumptions greatly simplify the dynamics of the troposphere through strong constraints acting on the thermodynamic profiles, which, in turn, implicitly separate the dynamics into horizontal and vertical components. The horizontal structure equations are akin to simpler Gill-like (1980) models, but with more precise definitions of the thermodynamically related parameters. Vertical structures are determined entirely by the thermodynamic reference profiles and lower and upper boundary conditions.

Here we summarize some essentials of the Yu and Neelin formulation. A primitive equation model is linearized about a continuously stratified basic state that assumes slow horizontal variations. The Betts–Miller scheme is employed to parameterize the collective effects of deep convection. Simplifications of the model come directly from the QE constraints implied by the Betts–Miller parameterization of the convective heating. A bulk formula is employed to parameterize surface moisture and sensible heat fluxes.

Under the QE constraints, the temperature and moisture perturbations are strongly constrained in the vertical and their magnitudes depend on the PBL moist enthalpy perturbation, h_b':

$$T' = A(p, x, y)h_b', \tag{A.1}$$

$$q' = \alpha\gamma A(p, x, y)h_b', \tag{A.2}$$

where $h_b' = T_b' + q_b'$ and α represents the degree of saturation (100% saturation when $\alpha = 1$) for the moisture reference profile. Notation $\gamma = (dq_{\text{sat}}/dT)|_{\bar{T}}$ denotes the saturation mixing ratio change with respect to temperature at a given level. Temperature and moisture perturbations are constrained in the vertical by $A(p, x, y)$, where A describes the three-dimensional dependence of the temperature reference profile given by (2.4a), (2.4b).

The momentum and moist static energy equations that govern small amplitude perturbations are expressed as

$$(\partial_t + \overline{\mathcal{D}}_m)\mathbf{V}_T' + \beta y\mathbf{k} \times \mathbf{V}_T' + \kappa\boldsymbol{\nabla}h_b' = 0, \tag{A.3}$$

$$[(\partial_t + \overline{\mathcal{D}}_T)A^* + \epsilon^*]h_b' + M\boldsymbol{\nabla}\cdot\mathbf{V}_T' = (1 + \gamma_0)\epsilon_b T_s', \tag{A.4}$$

where we have defined

$$\mathbf{V}'(x, y, p, t) = \mathbf{V}_T'(x, y, t)(A^+ - \widehat{A^+}), \tag{A.5}$$

$$\omega(x, y, p, t) = -\Omega(p)\boldsymbol{\nabla}\cdot\mathbf{V}(x, y, t), \tag{A.6}$$

$$A^* = \hat{A} + \widehat{\alpha\gamma A}, \tag{A.7}$$

and A^+ is defined in (2.2b). Vertical averages are given by

$$\widehat{(\,)} = \Delta p_t^{-1}\int_{p_t}^{p_0} (\,)\, dp$$

as in (2.2a). Here $\mathbf{V}_T$ denotes the wind vector associated with the QE baroclinic component and A^* provides a nondimensional measure of the thermal inertial of the motions associated with a given perturbation of PBL moist enthalpy, h_b. Two effects contribute to A^*: one from the temperature equation ($\hat{A}$); the other from the moisture equation $\widehat{\alpha\gamma A}$). In (A.3) and (A.4), $\overline{\mathcal{D}}_m$ and $\overline{\mathcal{D}}_T$ are two linear operators containing damping and advection terms for the momentum equation and moist static energy equation, respectively; ϵ^* is the collective thermal damping rate (including the Newtonian cooling and PBL moisture damping terms); M is the gross moist stability defined in (2.1a); and T_s' the SST perturbation.

The precipitation perturbation can be diagnostically derived from the moisture budget. For a steady-state case, this yields

$$P' = E' + \frac{\Delta p_t}{g}M_q\boldsymbol{\nabla}\cdot\mathbf{V}_T', \tag{A.8}$$

where M_q is the gross moisture stratification defined in (2.1b), E' is the local evaporation perturbation, Δp_t is the total pressure depth for deep convection, and g is the acceleration due to gravity.

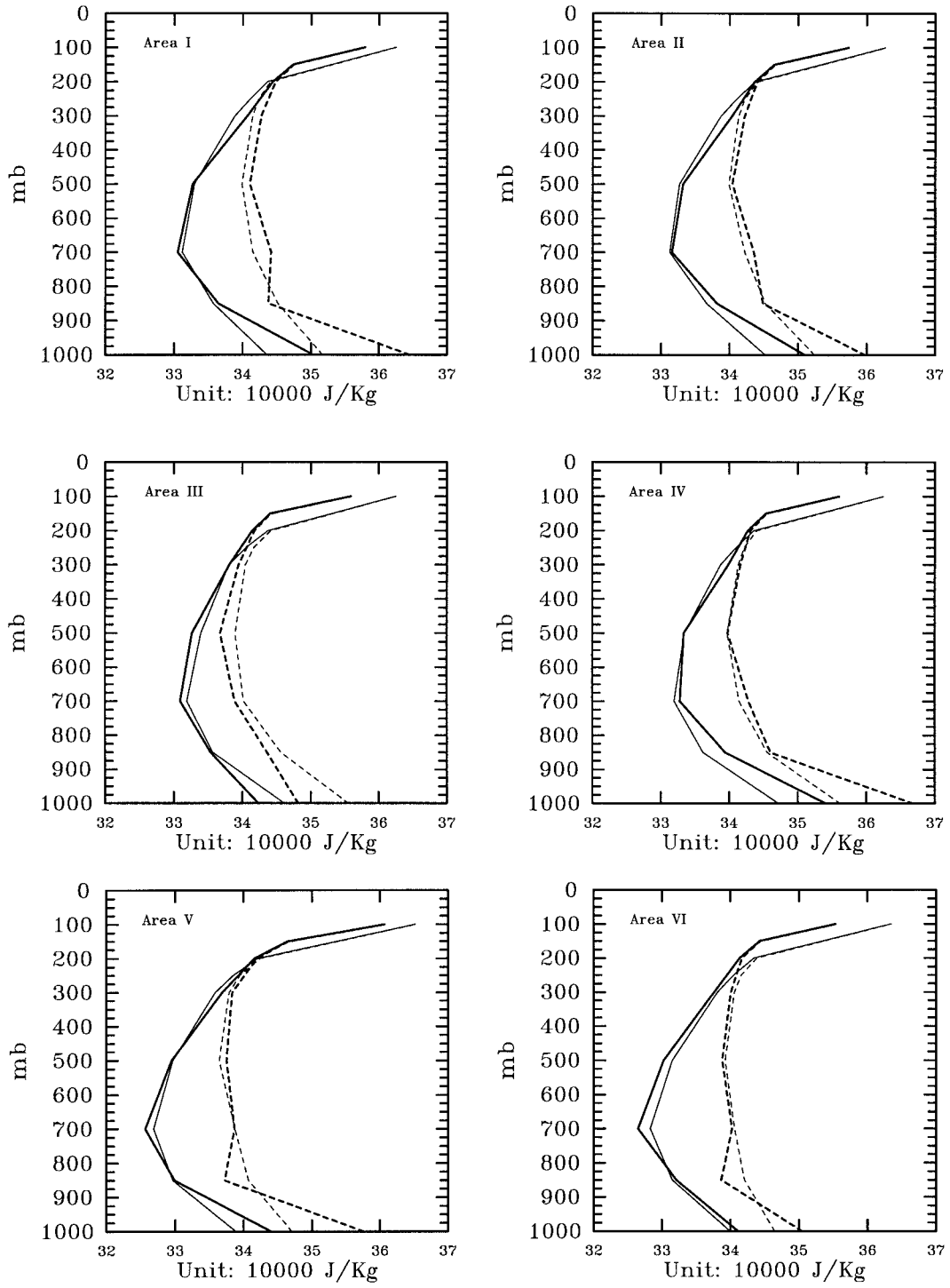

FIG. B1. As in Fig. 5 except for the comparison between rawinsonde soundings (heavy lines) and the NMC analyses (light lines).

APPENDIX B

ECMWF Data versus NMC Data

In section 4, we show results only from ECMWF data. Here a comparison between actual soundings and NMC analyses is shown in Fig. B1. Comparing this with Fig. 5, it is evident that, except in areas III and VI, the ECMWF soundings are significantly closer to the observed profiles than NMC soundings in the tropical Pacific, especially in the lower troposphere. Since esti-

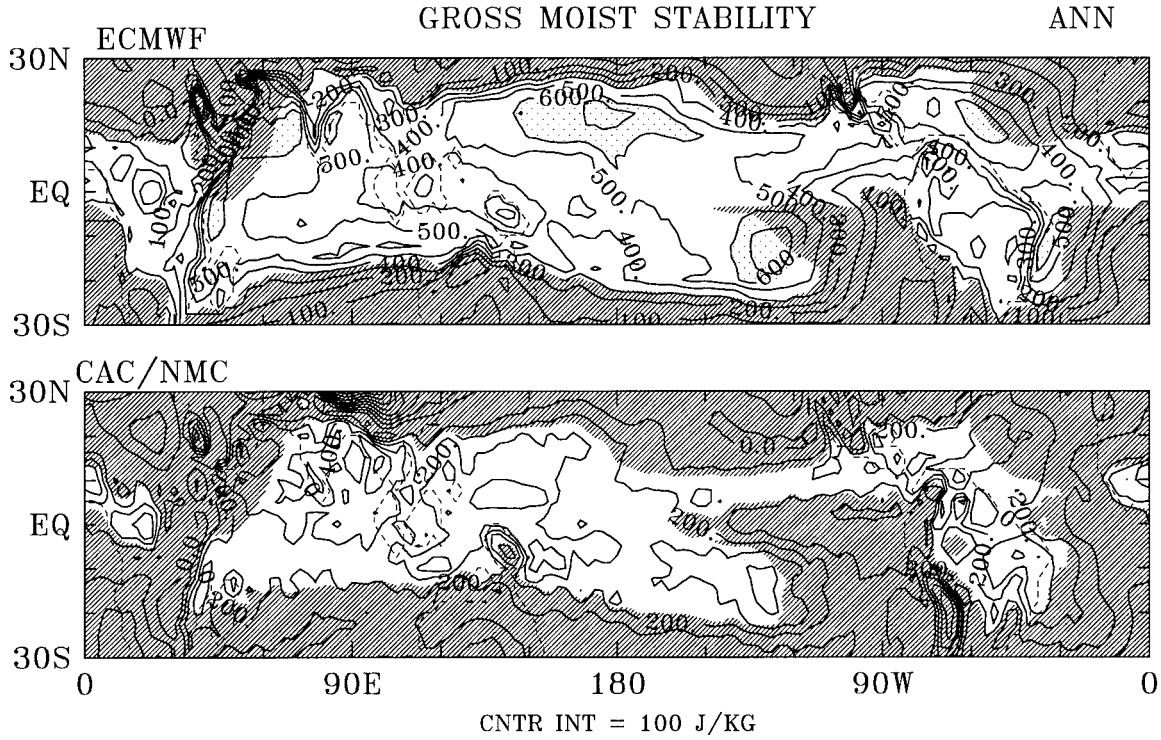

FIG. B2. Comparison of the gross moist stability (M) distribution between ECMWF analysis (upper panel) and NMC analysis (lower panel). Only the annual mean climatology is displayed here instead of the seasonal cycle case. Regions outside the domain of applicability are crosshatched. Contour interval 100 J Kg^{-1}; stippled over 600 J kg^{-1}.

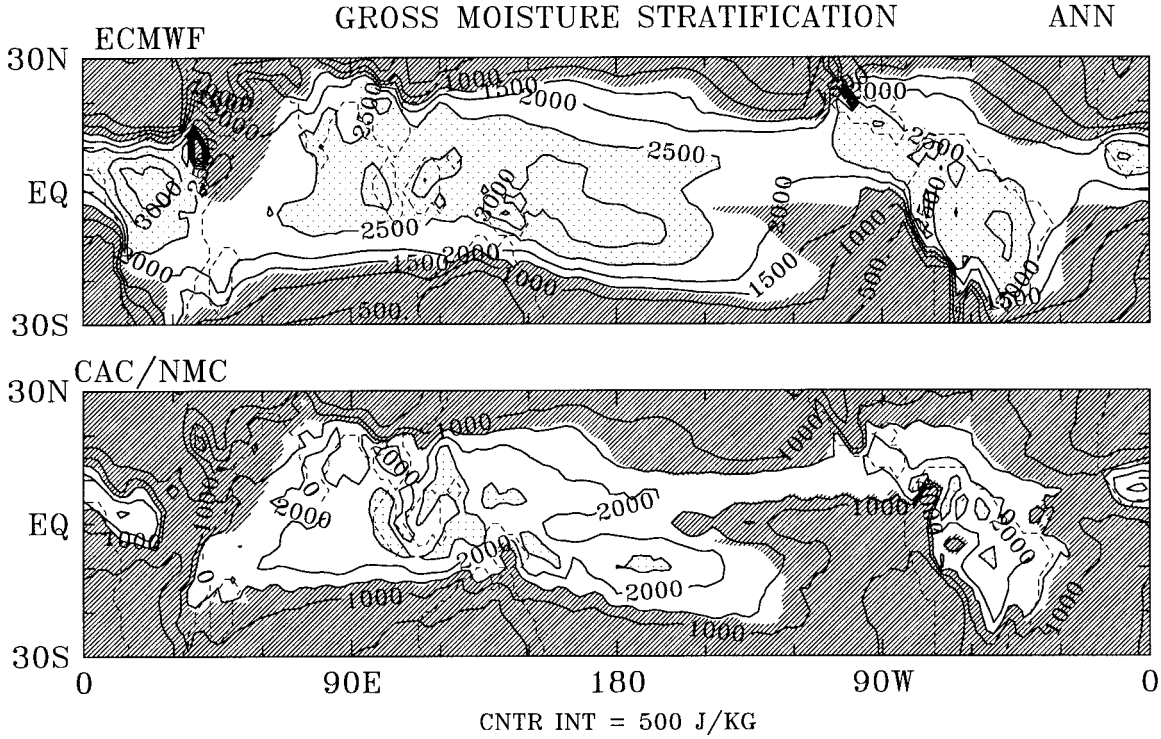

FIG. B3. As in Fig. B2 except for the gross moisture stratification (M_q) distribution. Contour interval 500 J Kg^{-1}; stippled over 2500 J kg^{-1}.

mates of M, M_q, and the maximum level of convection crucially depend on thermodynamic structures in the lower troposphere, this implies that the ECMWF data is a better choice to estimate the spatial distributions of the above quantities. We also note that the ECMWF data have a large bias in area III (tropical continents) due to large low-level moisture and temperature errors as we have discussed in section 4a.

Next, we compare the gross moist stability calculated, respectively, from ECMWF (upper panel) and NMC (lower panel) data in Fig. B2. Values of M calculated from NMC data are smaller than from ECMWF data; in most regions, less than 400 J Kg^{-1}. The field of M calculated from NMC analysis is smoother than from ECMWF analysis. Figure B3 shows the distributions of the gross moisture stratification calculated from the NMC analysis (the lower panel) and the ECMWF analysis (the upper panel), respectively. Similar to the results of Fig. B2, M_q calculated from NMC analysis has smaller values than from ECMWF analysis. Overall, however, the patterns from both analyses are similar.

Several possible effects may contribute to the differences in M and M_q between the NMC and the ECMWF analyses. First, NMC data only provide moisture data up to 500 mb while ECMWF data provide moisture data up to 100 mb. Second, it has been pointed out by several authors (Lambert 1988; Trenberth and Olson 1988) that due to different cumulus schemes used by NMC and ECMWF models, there are disagreements in the Tropics between these two models. Moreover, since the NMC data has a known error, which we have corrected with an iterative scheme (see section 3) we regard the ECMWF data as more reliable.

REFERENCES

Bengtsson, L., M. Kanamitsu, P. Kållberg, and S. Uppala, 1982: FGGE 4-dimensional data assimilation at ECMWF. *Bull. Amer. Meteor. Soc.,* **63,** 29–43.

Betts, A. K., 1986: A new convective adjustment scheme. Part I: Observational and theoretical basis. *Quart. J. Roy. Meteor. Soc.,* **112,** 677–691.

——, and M. J. Miller, 1986: A new convective adjustment scheme. Part II: Single column tests using GATE wave, BOMEX, ATEX and arctic air-mass data sets. *Quart. J. Roy. Meteor. Soc.,* **112,** 693–709.

Fu, R., A. D. DelGenio, and W. B. Rossow, 1990: Behavior of deep convection clouds in the tropical Pacific deduced from ISCCP radiances. *J. Climate,* **3,** 1129–1152.

——, ——, and ——, 1994: Influence of ocean surface conditions on atmospheric vertical thermodynamic structure and deep convection. *J. Climate,* **7,** 1092–1108.

Gill, A. E., 1980: Some simple solutions for heat-induced tropical circulation. *Quart. J. Roy. Meteor. Soc.,* **106,** 447–462.

Gutzler, D. S., and T. M. Wood, 1990: Structure of large-scale convective anomalies over tropical oceans. *J. Climate,* **3,** 483–496.

Hess, P. G., D. S. Battisti, and P. J. Rasch, 1993: The maintenance of the intertropical convergence zones and the large-scale tropical circulation on a water-covered earth. *J. Atmos. Sci.,* **50,** 691–713.

Jordan, C. L., 1958: Mean sounding for the West Indies area. *J. Meteor.,* **15,** 91–97.

Kleeman, R., 1991: A simple model of the atmospheric response to ENSO sea surface temperature anomalies. *J. Atmos. Sci.,* **48,** 3–18.

Lambert, S. J., 1988: A comparison of operational global analyses from the European Centre for Medium-Range Weather Forecasts (ECMWF) and the National Meteorological Center (NMC). *Tellus,* **40A,** 272–284.

Lau, K.-M., and L. Peng, 1987: Origin of low-frequency (intraseasonal) oscillations in the tropical atmosphere. Part I: Basic theory. *J. Atmos. Sci.,* **44,** 950–972.

——, and S. Shen, 1988: On the dynamics of intraseasonal oscillation and ENSO. *J. Atmos. Sci.,* **45,** 1781–1797.

Lindzen, R. S., and S. Nigam, 1987: On the role of sea surface temperature gradients in forcing low-level winds and convergence in the tropics. *J. Atmos. Sci.,* **44,** 2418–2436.

McPherson, R. D., K. H. Bergmam, R. E. Kistler, G. E. Rasch, and D. S. Gordon, 1979: The NMC operational global data assimilation system. *Mon. Wea. Rev.,* **107,** 1445–1461.

Neelin, J. D., 1997: Implications of convective quasi-equilbrium for the large-scale flow. *The Physics and Parameterization of Moist Atmospheric Convection,* R. K. Smith, Ed., Kluwer Academic, 413–446.

Neelin, J. D., and I. M. Held, 1987: Modeling tropical convergence based on the moist static energy budget. *Mon. Wea. Rev.,* **115,** 3–12.

——, and J.-Y. Yu, 1994: Modes of tropical variability under convective adjustment and the Madden–Julian oscillation. Part I: Analytical theory. *J. Atmos. Sci.,* **51,** 1876–1894.

——, I. M. Held, and K. H. Cook, 1987: Evaporation–wind feedback and low-frequency variability in the tropical atmosphere. *J. Atmos. Sci.,* **44,** 2341–2348.

Rasmusson, E. M., and T. H. Carpenter, 1982: Variations in tropical sea surface temperature and surface wind fields associated with the Southern Oscillation/El Niño. *Mon. Wea. Rev.,* **110,** 354–384.

Swinbank, R., T. N. Palmer, and M. K. Davey, 1988: Numerical simulations of the Madden–Julian oscillation. *J. Atmos. Sci.,* **45,** 774–788.

Trenberth, K. E., and J. G. Olson, 1988: An evaluation and intercomparison of global analyses from the National Meteorological Center and the European Centre for Medium-Range Weather Forecasts. *Bull. Amer. Meteor. Soc.,* **69,** 1047–1057.

Waliser, D. E., N. E. Graham, and C. Gautier, 1993: Comparison of highly reflective cloud and outgoing longwave radiation datasets for use in estimating tropical deep convection. *J. Climate,* **6,** 331–352.

Weare, B. C., 1986: A simple model of the tropical atmosphere with circulation dependent heating and specific humidity. *J. Atmos. Sci.,* **43,** 2001–2016.

Webster, O. J., 1981: Mechanisms determining the atmospheric response to sea surface temperature anomalies. *J. Atmos. Sci.,* **38,** 554–571.

Yu, J.-Y., and J. D. Neelin, 1994: Modes of tropical variability under convective adjustment and the Madden–Julian oscillation. Part II: Numerical results. *J. Atmos. Sci.,* **51,** 1895–1914.

——, and ——, 1997: Analytic approximations for moist convectively adjusted regions. *J. Atmos. Sci.,* **54,** 1054–1063.

Zebiak, S. E., 1982: A simple atmospheric model of relevance to El Niño. *J. Atmos. Sci.,* **39,** 2017–2027.

——, 1986: Atmospheric convergence feedback in a simple model for El Niño. *Mon. Wea. Rev.,* **114,** 1263–1271.

Zhang, C., 1993: Large-scale variability of atmospheric deep convection in relation to sea surface temperature in the tropics. *J. Climate,* **6,** 1898–1913.